Research Square

Preprints are preliminary reports that have not undergone peer review.
They should not be considered conclusive, used to inform clinical practice,
or referenced by the media as validated information.

Failure of Adaptive Frontoparietal Theta-Gamma Coupling Enhancement During Working Memory in Major Depressive Disorder

Xinyao Li
Tianjin University
Ying Gao
Tianjin Medical University
Wenquan Zhang
Tianjin University
Xue Tian
Tianjin Medical University
Meijuan Li
Tianjin Medical University
Shuang Liu
shuangliu@tju.edu.cn
Tianjin University
Dong Ming
Tianjin University

Research Article

Keywords: Major depressive disorder, Working memory, Theta-gamma phase-amplitude coupling, Cognitive impairment, Frontoparietal network, Electroencephalography

Posted Date: November 24th, 2026

DOI: https://doi.org/10.21203/rs.3.rs-11182274/v1

License: This work is licensed under a Creative Commons Attribution 4.0 International License.
Read Full License

Additional Declarations: No competing interests reported.

Failure of Adaptive Frontoparietal Theta-Gamma Coupling Enhancement During Working Memory in Major Depressive Disorder

Xinyao Li#[1], Ying Gao#[2], Wenquan Zhang[1], Xue Tian[2], Meijuan Li*[2], Shuang Liu*[1], Dong Ming[1]

[1] Academy of Medical Engineering and Translational Medicine, Tianjin University, Tianjin 300072, China.

[2] Mental Health Center, Tianjin Medical University, Tianjin 300222, China.

# Xinyao Li and Ying Gao contributed equally to this work and share first authorship.

* Correspondence:

Meijuan Li, Mental Health Center, Tianjin Medical University, 13 Liulin Road, Tianjin 300222, China. E-mail: meijuanli82@163.com.

Shuang Liu, Academy of Medical Engineering and Translational Medicine, Tianjin University, Tianjin 300072, China. E-mail: shuangliu@tju.edu.cn.

Abstract

Background: Working memory (WM) impairment is a core cognitive deficit in major depressive disorder (MDD), affecting learning and work abilities. Evidence from healthy individuals indicates that theta-gamma phase-amplitude coupling (TGC) supports WM organization and control. Characterizing MDDs' TGC during WM tasks may clarify the electrophysiological basis of impairment and guide future interventions.

Methods: Thirty-five MDD patients and thirty-five healthy controls (HC) completed low-/high-load (2-/4-back) numerical n-back tasks during EEG recording. WM performance was indexed by accuracy, d-prime, and reaction time. Long-range frontoparietal TGC was quantified by modulation index as frontal theta modulation of parietal gamma across left/right frontal-to-left/right parietal

pathways. Linear mixed-effects models tested group × load effects in performance, region-of-interest-averaged TGC, and frequency- and spatially resolved TGC. Regional power and theta-band weighted phase lag index were controls.

Results: MDDs showed significantly lower accuracy and d-prime than HCs only during the 4-back task ($p < 0.05$), indicating their high-load-dependent WM impairment. HCs showed higher region-of-interest-averaged TGC during the 4-back task than during the 2-back task across pathways ($p < 0.05$), whereas MDDs showed no difference between two tasks. MDDs also showed lower TGC than HCs in right-parietal pathways only during the 4-back task, indicating their impaired adaptive regulation of frontoparietal TGC with cognitive load. Widespread group × load interactions across theta-gamma frequencies and pathways ($p < 0.05$) further indicated a distributed frontoparietal TGC alteration in MDDs.

Conclusion: MDD shows impaired adaptive upregulation of frontoparietal TGC under high WM load, which may underlie WM impairment and inform future neuromodulation strategies.

Trial registration: Not applicable.

Keywords

Major depressive disorder; Working memory; Theta-gamma phase-amplitude coupling; Cognitive impairment; Frontoparietal network; Electroencephalography

Background

Major depressive disorder (MDD) is a prevalent and disabling psychiatric disorder that imposes substantial personal, social, and economic burden[1]. In addition to affective symptoms, cognitive dysfunction is increasingly recognized as a clinically meaningful feature of MDD[2–4]. Working memory (WM), the ability to maintain and manipulate goal-relevant information over short periods, is especially important because it supports learning, occupational performance, decision-making, and emotion regulation[5, 6]. WM impairment in MDD may persist even after mood symptoms improve,

limiting functional recovery and increasing vulnerability to relapse[7, 8]. Identifying the neural signatures of WM impairment is therefore important for understanding cognitive dysfunction in MDD and for developing mechanism-guided approaches to functional recovery.

A mechanistic account of WM impairment is also important because neural rhythms and network synchrony have become increasingly tractable targets for cognitive intervention. Non-invasive neuromodulation approaches, including repetitive transcranial magnetic stimulation (rTMS), theta-burst stimulation, and transcranial alternating-current stimulation (tACS), have been used to modulate WM-related neural activity and improve performance in healthy adults, older adults, and clinical populations with psychiatric disorders[9–13]. These studies suggest that WM performance can be shaped by targeting specific oscillatory and network mechanisms rather than by treating cognition only as a WM performance outcome. For MDD, identifying electrophysiological signatures associated with WM impairment and potentially accessible to rhythm-based modulation may provide a useful foundation for future precision interventions.

Theta-gamma phase-amplitude coupling (TGC) provides a promising electrophysiological mechanism linking WM computation with rhythmic neural control. As a form of cross-frequency coupling, TGC describes the modulation of high-frequency gamma amplitude by low-frequency theta phase, allowing neural activity at different temporal scales to be coordinated[14–16]. Theoretical models propose that theta cycles can organize multiple gamma events, thereby supporting the temporal ordering and maintenance of multiple WM representations[17–19]. Empirical evidence from animal electrophysiology, human intracranial recordings, and stimulation studies further supports a role for TGC in WM load, representational quality, and cognitive control over maintained information[20–23]. Thus, TGC is well positioned to serve as a mechanistic marker of how WM-related information is organized and controlled.

WM also depends on coordinated activity across the frontoparietal network. Frontal regions are closely involved in cognitive control, task-rule maintenance, and demand-related regulation, whereas parietal regions contribute to attentional selection and the maintenance of task-relevant

representations[6, 24–26]. Successful WM performance therefore requires dynamic coordination between frontal control signals and parietal representational activity. In this framework, long-range frontoparietal TGC, defined here as frontal theta phase modulation of parietal gamma amplitude, provides a network-level measure of cross-frequency coordination between control-related and representation-related regions. Characterizing this coupling across left and right frontoparietal pathways may help identify electrophysiological signatures associated with WM dysfunction in MDD and provide a network-level basis for future mechanism-guided intervention studies.

Here, we examined frontoparietal TGC during numerical n-back performance in patients with MDD and healthy controls. Using WM tasks with different cognitive demands, we evaluated whether frontoparietal TGC differed between groups and whether this coupling could provide an electrophysiological signature associated with WM dysfunction in MDD. We further characterized the frequency and spatial distribution of TGC effects and conducted control analyses of regional theta/gamma power and theta-band frontoparietal phase synchronization. By identifying frontoparietal coupling features associated with WM impairment, this study aimed to provide a mechanistic basis for future rhythm-based interventions.

Methods

Participants

Thirty-five patients with MDD and thirty-five healthy control (HC) participants were included in the study. Patients with MDD were recruited from the outpatient department of Tianjin Anning Hospital. HC participants were recruited from the community and Tianjin University through advertisements during the same period.

The general inclusion criteria for all participants were: age between 18 and 55 years; junior-high-school education or above; normal or corrected-to-normal vision and normal hearing; ability to read and understand the informed-consent form and self-report scales; and voluntary participation

with written informed consent. Patients in the MDD group were required to meet Diagnostic and Statistical Manual of Mental Disorders, Fifth Edition (DSM-5) diagnostic criteria for MDD, and the current depressive episode was independently confirmed by two attending-level psychiatrists or above.

The exclusion criteria were: psychiatric disorders other than MDD in the patient group or any DSM-5 psychiatric disorder in HC participants; history of head trauma or loss of consciousness; organic brain disease or severe physical illness; history of epileptic seizures or family history of epilepsy; and history of alcohol or psychoactive-substance dependence.

The study was conducted in accordance with the Declaration of Helsinki and was approved by the Ethics Committee of Tianjin Anding Hospital (Approval No. 2023-52). All participants provided written informed consent before the experiment.

Stimuli and Paradigm

Participants completed a numerical n-back WM task programmed in MATLAB R2019b and presented using Psychtoolbox-3[24, 27]. Visual stimuli were Arabic numerals from 1 to 9 presented in white on a black background (Figure 1). Each trial consisted of a 500 ms number presentation followed by a 2500 ms black-screen interval, yielding a total trial duration of 3000 ms.

The task included a low-load 2-back task and a high-load 4-back task. Each task was administered in a separate block of 60 trials and lasted approximately 180 s. The first n trials of each block were excluded from performance and EEG analyses because no correct n-back response could be defined for these trials.

Before each block, participants were informed of the current load level. During the task, they judged whether the current number matched the number presented n trials earlier. Participants pressed the "F" key for targets and the "J" key for non-targets. Targets and non-targets were presented in a pseudo-random order at a 1:1 ratio.

EEG Data Acquisition and Processing

EEG data were recorded using a Neuroscan SynAmps2 amplifier and a 64-channel Quik-Cap. Signals were acquired from 64 Ag/AgCl electrodes positioned according to the international 10-20 system. The left mastoid (M1) served as the online reference. The sampling rate was 1000 Hz, and electrode impedance was maintained below 10 kΩ throughout recording.

Offline preprocessing was performed in MATLAB R2019 using EEGLAB[28]. Continuous EEG data were re-referenced to the average of the bilateral mastoids, downsampled to 500 Hz, and band-pass filtered from 0.5 to 120 Hz. Independent component analysis, combined with the ADJUST plugin, was used to identify and remove components reflecting eye blinks, eye movements, and electromyographic artifacts[29]. EEG data were epoched from 500 ms before stimulus onset to 3000 ms after stimulus onset, and the -500 to 0 ms prestimulus interval was used for baseline correction. Epochs with obvious residual artifacts were removed by visual inspection. Except for CB1 and CB2, all 60 scalp channels were retained for subsequent analyses.

WM Performance Measures

WM performance was indexed by accuracy, d-prime, and correct-response reaction time. Accuracy was calculated as the proportion of correct responses across target and non-target trials. d-prime was used as a signal-detection index of response sensitivity and was calculated as the z-transformed hit rate minus the z-transformed false-alarm rate[30]. Hit rates or false-alarm rates of 0 or 1 were adjusted before z transformation to avoid infinite d-prime estimates[31]. Correct-response reaction time was calculated in milliseconds using only trials with correct responses.

Frontoparietal ROI Definition

Because the frontoparietal network is central to WM control and storage, four anatomical electrode regions were predefined[6, 24]. The left frontal region (LF) included FP1, AF3, F7, F5, F3,

F1, FC5, FC3, FC1, and C1. The right frontal region (RF) included FP2, AF4, F2, F4, F6, F8, FC2, FC4, FC6, and C2. The left parietal region (LP) included C5, C3, CP5, CP3, CP1, P7, P5, P3, and P1. The right parietal region (RP) included C4, C6, CP2, CP4, CP6, P2, P4, P6, and P8.

These regions were combined to define four long-range frontoparietal pathways: LF-LP, LF-RP, RF-LP, and RF-RP. For each pathway, TGC was calculated for all frontal-parietal channel pairs, yielding 10 × 9 channel pairs per pathway.

TGC Analysis

Long-range theta-gamma phase-amplitude coupling (TGC) was quantified using the modulation index (MI) proposed by Tort et al[32]. MI estimates the degree to which high-frequency gamma amplitude is non-uniformly distributed across low-frequency theta phase, with higher MI values indicating stronger phase-amplitude coupling.

For each frontal-parietal channel pair, the frontal signal was used to extract theta phase and the parietal signal was used to extract gamma amplitude (Figure 2). Theta phase was extracted from 4-8 Hz in 1 Hz steps, yielding five theta frequencies. Gamma amplitude was extracted from 30-100 Hz in 5 Hz steps, yielding 15 gamma frequencies. For each theta-gamma pair, the Hilbert transform was used to obtain the instantaneous theta phase and gamma amplitude envelope during the 0-3000 ms post-stimulus task period. Gamma amplitude values were sorted into 18 theta phase bins and normalized to form a phase-amplitude distribution. MI was then calculated by quantifying the normalized Kullback-Leibler divergence between the observed phase-amplitude distribution and a uniform distribution[33, 34].

This procedure yielded a 10 × 9 × 5 × 15 TGC matrix for each participant, load task, and frontoparietal pathway. TGC was then summarized at three levels. First, region-of-interest (ROI)-averaged TGC was obtained by averaging across all channel pairs and theta-gamma frequency pairs within each pathway, yielding one TGC value per participant, load task, and pathway. Second, frequency-resolved TGC was obtained by averaging across channel pairs while preserving the 5 × 15

theta-gamma frequency space. Third, spatially resolved TGC was obtained by averaging across theta-gamma frequency pairs while preserving the 10 × 9 frontal-parietal channel-pair space.

PSD and Theta-wPLI Control Analyses

To evaluate whether the TGC findings could be explained by single-frequency power differences, regional power was analyzed in the frequency bands and regions corresponding to the direction of the TGC calculation. Theta power was analyzed in the left and right frontal regions (4-8 Hz), and gamma power was analyzed in the left and right parietal regions (30-100 Hz). Power spectral density was computed in MATLAB using the pwelch function with a 512-sample Hamming window and 50% overlap[35]. Power values were averaged across electrodes within each ROI and frequency band for each participant and load task.

To evaluate whether the TGC findings could be explained by theta-band phase synchronization, weighted phase lag index (wPLI) was computed for theta-band activity (4-8 Hz) in the same four frontoparietal pathways. wPLI was used because it reduces sensitivity to zero-lag synchronization caused by common sources or volume conduction[36]. For each pathway, wPLI was calculated across all cross-regional channel pairs and averaged to obtain one theta-wPLI value per participant and load task.

Statistical Analysis

Demographic and clinical variables were analyzed according to variable type. Continuous variables were reported as median and interquartile range and compared between groups using Mann-Whitney U tests. Sex distribution was compared using a chi-square test, and handedness was compared using Fisher's exact test. Demographic and clinical comparisons were used to characterize the sample and were reported with uncorrected p values.

WM performance and electrophysiological outcomes were analyzed using linear mixed-effects models in MATLAB. For each dependent variable, group (MDD, HC), load (2-back, 4-back), and the

group × load interaction was entered as fixed effects. Subject was modeled as a random effect with a subject-specific load slope, using the model Y ~ Group × Load + (1 + Load | Subject_ID). Models were fit using restricted maximum likelihood with reference coding for categorical predictors. Degrees of freedom for fixed-effect tests and model-based contrasts were estimated using the Satterthwaite method[37, 38].

For significant group × load interactions, follow-up simple effects were used to characterize the interaction direction. These included within-group load effects (4-back - 2-back) separately for MDD and HC participants, and between-group effects (HC - MDD) separately at 2-back and 4-back. Interaction effects were summarized as Δinteraction = (HC_4-back - HC_2-back) - (MDD_4-back - MDD_2-back). Positive Δinteraction values therefore indicate larger load-related increases in HC than in MDD.

False-discovery-rate (FDR) correction was performed using the Benjamini-Hochberg procedure[39]. For WM performance analyses, the primary interaction tests were corrected across the three primary WM performance outcomes: accuracy, d-prime, and correct-response reaction time. ROI-averaged TGC interactions were corrected across the four frontoparietal pathways. Frequency-resolved TGC analyses were corrected within each pathway across 75 theta-gamma frequency pairs. Spatially resolved TGC analyses were corrected within each pathway across 90 frontal-parietal channel pairs. Control analyses were corrected separately across the four regional power measures and the four theta-wPLI pathway measures. Statistical significance was defined as $q < 0.05$ after FDR correction.

Results

Participant Characteristics

The study included 35 patients with MDD and 35 age- and sex-matched HC participants. Demographic and clinical characteristics are summarized in Table 1. The groups did not differ

significantly in sex distribution (χ^2 (1) = 1.447, p = 0.229), age (U = 529.5, p = 0.330), years of education (U = 601.5, p = 0.900), or handedness (Fisher exact p = 1.000). Clinically, MDD participants showed significantly higher PHQ-9[40] scores (U = 11.0, p < 0.001) and GAD-7[41] scores (U = 34.0, p < 0.001), indicating greater depressive and anxiety symptom burden in the clinical group. HCL-32[42] scores did not differ significantly between groups (U = 461.0, p = 0.074), consistent with the absence of elevated hypomanic symptoms in the MDD group.

Load-Dependent WM Performance Impairment in MDD

Linear mixed-effects models revealed significant group × load interaction for accuracy and d-prime when comparing the MDD and HC groups across different working memory loads (Figure 3; Accuracy: F (1, 68) = 10.02, p = 0.002, q = 0.0069; d-prime: F (1, 68) = 4.77, p = 0.032, q = 0.049). Post hoc simple-effects analyses showed that, during the 4-back task, the MDD group had significantly lower accuracy and d-prime than the HC group (Accuracy: HC - MDD = 0.145, q < 0.001; d-prime: HC - MDD = 0.765, q < 0.001), whereas no significant group differences were observed during the 2-back task (Accuracy: HC - MDD = 0.041, q = 0.567; d-prime: HC - MDD = 0.321, q = 0.567). Within-group paired comparisons further indicated that accuracy (MDD: 0.787 ± 0.121 to 0.580 ± 0.137, Δ4-back-2-back = -0.208, q < 0.001; HC: 0.828 ± 0.129 to 0.725 ± 0.106, Δ4-back-2-back = -0.104, q < 0.001) and d-prime (MDD: 2.313 ± 0.814 to 1.059 ± 0.608, Δ4-back-2-back = -1.254, q < 0.001; HC: 2.634 ± 1.013 to 1.824 ± 0.944, Δ4-back-2-back = -0.810, q < 0.001) decreased with increasing task load in both groups. In contrast, correct-response reaction time did not show a significant group × load interaction (F (1, 68) = 0.07, p = 0.785, q = 0.785). These findings suggest that WM impairment in MDD is load-dependent, primarily reflected in reduced accuracy and signal discrimination under high-load tasks, while reaction time did not exhibit a corresponding group-difference pattern.

Failure of Load-Related Frontoparietal TGC Enhancement in MDD

We next examined group × load interactions in ROI-averaged frontoparietal TGC across the four predefined pathways. Significant interactions were observed in all four pathways after FDR correction (Figure 4): LF-LP, $F(1, 59) = 8.22$, $p = 0.006$, $q = 0.008$; LF-RP, $F(1, 58) = 15.79$, $p < 0.001$, $q < 0.001$; RF-LP, $F(1, 60) = 6.85$, $p = 0.011$, $q = 0.011$; and RF-RP, $F(1, 59) = 16.23$, $p < 0.001$, $q < 0.001$. To characterize these interactions, we conducted follow-up simple-effects analyses (Table S1). These analyses showed no significant group differences in TGC during the 2-back task (all $q \geq 0.139$). During the 4-back task, however, the MDD group showed significantly lower TGC than the HC group in pathways involving the right parietal ROI, namely LF-RP (HC - MDD = 0.001212, $q = 0.011$) and RF-RP (HC - MDD = 0.001178, $q = 0.011$). Within-group paired comparisons further showed that TGC was significantly higher during the 4-back task than during the 2-back task in all four pathways in the HC group (all $q \leq 0.002$), whereas no significant tasks difference was observed in the MDD group (all $q \geq 0.196$). These findings suggest a failure of adaptive load-related enhancement of frontoparietal TGC in MDD, with the most evident high-load abnormalities occurring in pathways involving the right parietal ROI.

Broad Frequency Distribution of TGC Interaction Effects

To determine whether the ROI-averaged interaction effects were concentrated in specific theta-gamma frequency pairs, we averaged TGC across channel pairs within each ROI and tested the group × load interaction separately for each theta-gamma frequency pair. Significant interactions were broadly distributed across the theta-gamma frequency space (Figure 5 and Table 2). After FDR correction within each pathway, significant interactions were observed in 74 of 75 frequency pairs for LF-LP, 75 of 75 for LF-RP, 71 of 75 for RF-LP, and 75 of 75 for RF-RP. In all four pathways, the mean and median Δinteraction values were positive, indicating that the frequency-resolved effects consistently reflected greater load-related TGC enhancement in HC than in MDD. Together, these

results indicate that the ROI-averaged TGC abnormality reflected a broadly distributed theta-gamma coupling effect across the tested theta-gamma frequency pairs.

Broad Spatial Distribution of TGC Interaction Effects

To determine whether the TGC interaction effects were spatially concentrated in specific frontoparietal channel pairs, we also averaged TGC across theta-gamma frequency pairs and tested the group × load interaction separately for each channel pair within each ROI. Significant interactions were observed in most channel pairs within each pathway after FDR correction (Figure 6 and Table 2): 88 of 90 channel pairs for LF-LP, 89 of 90 for LF-RP, 85 of 90 for RF-LP, and 90 of 90 for RF-RP. The mean and median Δinteraction values were also positive in all four pathways, indicating consistently greater load-related TGC enhancement in the HC group than in the MDD group across channel pairs. For visualization, Figure 6 displays the strongest 10% of FDR-significant channel-pair effects within each pathway, whereas the complete channel-pair matrices are shown in Figure S1. Together, these spatially resolved results indicate that abnormal load-dependent TGC modulation in MDD was broadly distributed across frontoparietal channel pairs.

Independence of TGC Abnormalities from Power and Phase Synchronization Effects

Finally, we tested whether the TGC findings were accompanied by group × load effects in regional theta/gamma power or theta-band frontoparietal phase synchronization. Regional power analyses showed no significant group × load interactions after FDR correction for left frontal theta power, right frontal theta power, left parietal gamma power, or right parietal gamma power (all $q \geq 0.203$; Figure 7 and Table S2). Left parietal gamma power showed a weak uncorrected trend, but this effect did not survive FDR correction and its Δinteraction value was negative, in contrast to the consistently positive TGC interaction effects.

Theta-band wPLI analyses likewise showed no significant group × load interactions in any of the four frontoparietal pathways (all $q = 0.650$; Figure 7 and Table S2). Together, these control

analyses indicate that the observed TGC abnormalities occurred without corresponding group × load effects in regional theta/gamma power or theta-band frontoparietal phase synchronization.

Discussion

This study examined load-dependent frontoparietal TGC during WM processing in MDD. The findings showed a consistent pattern of load-dependent dysfunction at both behavioral and neural levels. Behaviorally, the MDD group showed greater impairment in accuracy and d-prime under high WM load, without a corresponding group difference in correct-response reaction time. Neurally, the HC group showed adaptive enhancement of frontoparietal TGC as WM load increased, whereas this modulation was blunted in the MDD group, particularly in pathways involving the right parietal region during the 4-back task. Frequency- and spatially resolved analyses indicated that these effects were broadly distributed across theta-gamma frequency pairs and frontoparietal channel pairs. Control analyses further suggested that the TGC findings were not driven by regional theta/gamma power or theta-band frontoparietal phase synchronization. Together, these findings suggest that impaired load-adaptive frontoparietal cross-frequency coordination may be a key neural mechanism underlying WM impairment in MDD.

The WM performance findings indicate that increasing WM load placed a disproportionate demand on MDD participants. Accuracy and d-prime decreased from 2-back to 4-back in both groups, consistent with the expected effect of greater n-back difficulty, but the decline was larger in the MDD group. This profile fits with evidence that cognitive deficits in the MDD group become more apparent when task demands increase and available control resources are taxed[2, 8, 43, 44]. Reaction time did not show the same interaction pattern, suggesting that the WM performance impairment was expressed mainly as reduced response accuracy and sensitivity rather than generalized slowing. The electrophysiological findings therefore occurred in a task context in which MDD participants also showed greater load-related performance impairment.

The central neural finding was a group difference in the way frontoparietal TGC adapted to WM

load. In the HC group, TGC increased from the 2-back task to the 4-back task across all four pathways. This load-related enhancement may reflect an adaptive coordination process in which frontal theta phase organizes parietal gamma activity to support the maintenance and control of task-relevant representations[18, 21, 22]. In the MDD group, the absence of comparable TGC enhancement suggests reduced flexibility in coordinating frontal control signals with parietal representational activity as cognitive demand increases. The pattern therefore points to an abnormal regulation of TGC rather than a global loss of coupling. The additional high-load group differences in right-parietal pathways indicate that this blunted regulation was especially evident when task demand was highest[45, 46].

Frequency- and spatially resolved analyses convergently revealed a broadly distributed group × load interaction in frontoparietal TGC across both spectral and spatial dimensions. At the frequency level, the widespread spectral profile indicates that the ROI-level findings reflect a global alteration in load-dependent cross-frequency coordination, consistent with theoretical models framing working memory as reliant on flexible cross-temporal coordination via theta-gamma nested oscillations[14, 15, 17]. Spatially, significant interactions emerged across most channel pairs within all predefined frontoparietal pathways, confirming that the observed TGC dysregulation represents a distributed network-level impairment affecting the entire frontoparietal system. Notably, high-load group differences were most pronounced in pathways involving the right parietal region, in line with the established role of right frontoparietal systems in attentional monitoring, cognitive control, and demand-related processing[47–49] , suggesting that right parietal coupling dysfunction may be a particularly prominent facet of the broader frontoparietal regulation deficit in MDD.

The control analyses provide further support for interpreting the main effect at the level of cross-frequency coordination. Regional theta and gamma power did not show significant group × load interactions after correction, and theta-band wPLI showed no significant interaction in any frontoparietal pathway. These findings suggest that the TGC abnormality was not driven by regional single-frequency power or theta-band phase synchronization alone. Instead, the effect was most

clearly expressed in the relationship between frontal theta phase and parietal gamma amplitude. This specificity is important because it places the MDD-related alteration at the level of cross-frequency network coordination, a process that may be especially relevant for integrating control and representational components of working memory[36, 50–52].

These findings may inform mechanism-guided interventions targeting cognitive dysfunction in MDD. Rhythmic neuromodulation approaches aim to improve cognition by modulating oscillatory synchrony and cross-frequency coordination[9–11, 53]. By identifying reduced adaptive enhancement of frontoparietal TGC under high cognitive demand, the present study suggests frontoparietal TGC as a candidate marker for future rhythm-based intervention research, although intervention effects were not tested directly.

Several limitations should be noted. The moderate sample size requires replication in larger cohorts, and the cross-sectional design precludes causal inference. Future longitudinal and intervention studies should test whether abnormal TGC regulation predicts WM impairment, symptom improvement, or treatment response. EEG's limited spatial specificity also warrants validation with source localization or multimodal imaging. Finally, medication status, illness history, symptom severity, and anxiety comorbidity may influence cognitive and electrophysiological measures, requiring studies in more clinically specific cohorts.

Conclusions

In summary, patients with MDD showed greater WM impairment under high load and reduced adaptive enhancement of frontoparietal TGC during WM. This abnormal regulation was broadly expressed across theta-gamma frequency pairs and frontoparietal channel pairs and was not explained by regional theta/gamma power or theta-band phase synchronization. These findings suggest that impaired load-adaptive frontoparietal cross-frequency coordination may represent an electrophysiological signature of WM dysfunction in MDD and inform future rhythm-based cognitive interventions.

List of abbreviations

EEG, electroencephalography; FDR, false discovery rate; HC, healthy control; LF, left frontal; LP, left parietal; MDD, major depressive disorder; MI, modulation index; PSD, power spectral density; RF, right frontal; ROI, region of interest; RP, right parietal; TGC, theta-gamma phase-amplitude coupling; WM, working memory; wPLI, weighted phase lag index.

Declarations

Ethics approval and consent to participate

The study was conducted in accordance with the Declaration of Helsinki and was approved by the Ethics Committee of Tianjin Anning Hospital (Approval No. 2023-52). All participants provided written informed consent before participation.

Consent for publication

Not applicable. The manuscript does not contain data from any individually identifiable person.

Availability of data and materials

The datasets generated and/or analyzed during the current study are not publicly available due to privacy and ethical restrictions involving participant data but are available from the corresponding author on reasonable request.

Competing interests

The authors declare that they have no competing interests.

Funding

This work was supported by the National Natural Science Foundation of China (Grant No.

62376187) and the Tianjin Science and Technology Program, Major Special Project and Engineering (Grant No. 25ZXWCSY00310).

Authors' contributions

XL: Conceptualization, Methodology, Formal analysis, Software, Visualization, Writing - original draft. YG: Investigation, Data curation, Writing - review and editing. WZ: Formal analysis, Software, Visualization, Writing - review and editing. XT: Investigation, Data curation, Writing - review and editing. ML: Resources, Supervision, Project administration, Writing - review and editing. SL: Conceptualization, Methodology, Supervision, Writing - original draft, Writing - review and editing. DM: Supervision, Resources, Writing - review and editing. All authors read and approved the final manuscript.

Acknowledgements

The authors thank all participants for their involvement in the study.

Reference

1. Vos T, Lim SS, Abbafati C, Abbas KM, Abbasi M, Abbasifard M, et al. Global burden of 369 diseases and injuries in 204 countries and territories, 1990–2019: a systematic analysis for the global burden of disease study 2019. The Lancet. 2020;396:1204-22. doi:10.1016/S0140-6736(20)30925-9.

2. Snyder HR. Major depressive disorder is associated with broad impairments on neuropsychological measures of executive function: a meta-analysis and review. Psychol. Bull. 2013;139:81-132. doi:10.1037/a0028727.

3. Semkovska M, Quinlivan L, O'Grady T, Johnson R, Collins A, O'Connor J, et al. Cognitive function following a major depressive episode: a systematic review and meta-analysis. Lancet Psychiatry. 2019;6:851-61. doi:10.1016/S2215-0366(19)30291-3.

409 4. Rock PL, Roiser JP, Riedel WJ, Blackwell AD. Cognitive impairment in depression: a
410 systematic review and meta-analysis. Psychol. Med. 2014;44:2029-40.
411 doi:10.1017/S0033291713002535.
412 5. Baddeley A. Working memory: looking back and looking forward. Nat. Rev. Neurosci.
413 2003;4:829-39. doi:10.1038/nrn1201.
414 6. D'Esposito M, Postle BR. The cognitive neuroscience of working. Annu. Rev. Psychol.
415 2015;66:115-42. doi:10.1146/annurev-psych-010814-015031.
416 7. McIntyre RS, Cha DS, Soczynska JK, Woldeyohannes HO, Gallaugher LA, Kudlow P, et al.
417 Cognitive deficits and functional outcomes in major depressive disorder: determinants, substrates,
418 and treatment interventions. Depress. Anxiety. 2013;30:515-27. doi:10.1002/da.22063.
419 8. Nikolin S, Tan YY, Schwaab A, Moffa A, Loo CK, Martin D. An investigation of working
420 memory deficits in depression using the n-back task: a systematic review and meta-analysis. J.
421 Affect. Disord. 2021;284:1-8. doi:10.1016/j.jad.2021.01.084.
422 9. Reinhart RMG, Nguyen JA. Working memory revived in older adults by synchronizing
423 rhythmic brain circuits. Nat. Neurosci. 2019;22:820-7. doi:10.1038/s41593-019-0371-x.
424 10. Violante IR, Li LM, Carmichael DW, Lorenz R, Leech R, Hampshire A, et al. Externally
425 induced frontoparietal synchronization modulates network dynamics and enhances working
426 memory performance. eLife. 2017;6:e22001. doi:10.7554/eLife.22001.
427 11. Polanía R, Nitsche MA, Korman C, Batsikadze G, Paulus W. The importance of timing in
428 segregated theta phase-coupling for cognitive performance. Curr. Biol. 2012;22:1314-8.
429 doi:10.1016/j.cub.2012.05.021.
430 12. Alekseichuk I, Turi Z, Amador de Lara G, Antal A, Paulus W. Spatial working memory in
431 humans depends on theta and high gamma synchronization in the prefrontal cortex. Curr. Biol. CB.
432 2016;26:1513-21. doi:10.1016/j.cub.2016.04.035.
433 13. Vosskuhl J, Huster RJ, Herrmann CS. Increase in short-term memory capacity induced by
434 down-regulating individual theta frequency via transcranial alternating current stimulation. Front.

435 Hum. Neurosci. 2015;9. doi:10.3389/fnhum.2015.00257.
436 14. Canolty RT, Knight RT. The functional role of cross-frequency coupling. Trends Cogn. Sci.
437 2010;14:506-15. doi:10.1016/j.tics.2010.09.001.
438 15. Jensen O, Colgin LL. Cross-frequency coupling between neuronal oscillations. Trends Cogn.
439 Sci. 2007;11:267-9. doi:10.1016/j.tics.2007.05.003.
440 16. Lisman JE, Jensen O. The theta-gamma neural code. Neuron. 2013;77:1002-16.
441 doi:10.1016/j.neuron.2013.03.007.
442 17. Miller EK, Lundqvist M, Bastos AM. Working memory 2.0. Neuron. 2018;100:463-75.
443 doi:10.1016/j.neuron.2018.09.023.
444 18. Lisman JE, Idiart MAP. Storage of 7 ± 2 short-term memories in oscillatory subcycles.
445 Science. 1995;267:1512-5. doi:10.1126/science.7878473.
446 19. Jensen O. Maintenance of multiple working memory items by temporal segmentation.
447 Neuroscience. 2006;139:237-49. doi:10.1016/j.neuroscience.2005.06.004.
448 20. Li S, Bai W, Liu T, Yi H, Tian X. Increases of theta–low gamma coupling in rat medial
449 prefrontal cortex during working memory task. Brain Res. Bull. 2012;89:115-23.
450 doi:10.1016/j.brainresbull.2012.07.012.
451 21. Axmacher N, Henseler MM, Jensen O, Weinreich I, Elger CE, Fell J. Cross-frequency
452 coupling supports multi-item working memory in the human hippocampus. Proc. Natl. Acad. Sci.
453 2010;107:3228-33. doi:10.1073/pnas.0911531107.
454 22. Daume J, Kamiński J, Schjetnan AGP, Salimpour Y, Khan U, Kyzar M, et al. Control of
455 working memory by phase–amplitude coupling of human hippocampal neurons. Nature.
456 2024;629:393-401. doi:10.1038/s41586-024-07309-z.
457 23. Lundqvist M, Herman P, Warden MR, Brincat SL, Miller EK. Gamma and beta bursts during
458 working memory readout suggest roles in its volitional control. Nat. Commun. 2018;9:394.
459 doi:10.1038/s41467-017-02791-8.
460 24. Owen AM, McMillan KM, Laird AR, Bullmore E. N-back working memory paradigm: a

461 meta-analysis of normative functional neuroimaging studies. Hum. Brain Mapp. 2005;25:46-59.
462 doi:10.1002/hbm.20131.
463 25. Rottschy C, Langner R, Dogan I, Reetz K, Laird AR, Schulz JB, et al. Modelling neural
464 correlates of working memory: a coordinate-based meta-analysis. Neuroimage. 2012;60:830-46.
465 doi:10.1016/j.neuroimage.2011.11.050.
466 26. Wager TD, Smith EE. Neuroimaging studies of working memory: a meta-analysis. Cogn.
467 Affect. Behav. Neurosci. 2003;3:255-74. doi:10.3758/cabn.3.4.255.
468 27. Brainard DH. The psychophysics toolbox. Spat. Vis. 1997;10:433-6.
469 28. Delorme A, Makeig S. EEGLAB: an open source toolbox for analysis of single-trial eeg
470 dynamics including independent component analysis. J. Neurosci. Methods. 2004;134:9-21.
471 doi:10.1016/j.jneumeth.2003.10.009.
472 29. Mognon A, Jovicich J, Bruzzone L, Buiatti M. ADJUST: an automatic eeg artifact detector
473 based on the joint use of spatial and temporal features. Psychophysiology. 2011;48:229-40.
474 doi:10.1111/j.1469-8986.2010.01061.x.
475 30. Stanislaw H, Todorov N. Calculation of signal detection theory measures. Behav. Res.
476 Methods Instrum. Comput. J. Psychon. Soc. Inc. 1999;31:137-49. doi:10.3758/bf03207704.
477 31. Hautus MJ. Corrections for extreme proportions and their biasing effects on estimated values
478 ofd′. Behav. Res. Methods Instrum. Comput. 1995;27:46-51. doi:10.3758/BF03203619.
479 32. Tort ABL, Komorowski R, Eichenbaum H, Kopell N. Measuring phase-amplitude coupling
480 between neuronal oscillations of different frequencies. J. Neurophysiol. 2010;104:1195-210.
481 doi:10.1152/jn.00106.2010.
482 33. Canolty RT, Edwards E, Dalal SS, Soltani M, Nagarajan SS, Kirsch HE, et al. High gamma
483 power is phase-locked to theta oscillations in human neocortex. Science. 2006;313:1626-8.
484 doi:10.1126/science.1128115.
485 34. Cohen MX. Assessing transient cross-frequency coupling in eeg data. J. Neurosci. Methods.
486 2008;168:494-9. doi:10.1016/j.jneumeth.2007.10.012.

487 35. Welch P. The use of fast fourier transform for the estimation of power spectra: a method based
488 on time averaging over short, modified periodograms. IEEE Trans. Audio Electroacoustics.
489 1967;15:70-3. doi:10.1109/TAU.1967.1161901.
490 36. Vinck M, Oostenveld R, Wingerden M van, Battaglia F, Pennartz CMA. An improved index of
491 phase-synchronization for electrophysiological data in the presence of volume-conduction, noise
492 and sample-size bias. NeuroImage. 2011;55:1548-65. doi:10.1016/j.neuroimage.2011.01.055.
493 37. Gueorguieva R, Krystal JH. Move over anova: progress in analyzing repeated-measures data
494 and its reflection in papers published in the archives of general psychiatry. Arch. Gen. Psychiatry.
495 2004;61:310-7. doi:10.1001/archpsyc.61.3.310.
496 38. Barr DJ, Levy R, Scheepers C, Tily HJ. Random effects structure for confirmatory hypothesis
497 testing: keep it maximal. J. Mem. Lang. 2013;68:255-78. doi:10.1016/j.jml.2012.11.001.
498 39. Benjamini Y, Hochberg Y. Controlling the false discovery rate: a practical and powerful
499 approach to multiple testing. J. R. Stat. Soc. Ser. B Methodol. 1995;57:289-300. doi:10.1111/j.2517-
500 6161.1995.tb02031.x.
501 40. Costantini L, Pasquarella C, Odone A, Colucci ME, Costanza A, Serafini G, et al. Screening
502 for depression in primary care with patient health questionnaire-9 (phq-9): a systematic review. J.
503 Affect. Disord. 2021;279:473-83. doi:10.1016/j.jad.2020.09.131.
504 41. Spitzer RL, Kroenke K, Williams JBW, Löwe B. A brief measure for assessing generalized
505 anxiety disorder: the gad-7. Arch. Intern. Med. 2006;166:1092-7. doi:10.1001/archinte.166.10.1092.
506 42. Angst J, Adolfsson R, Benazzi F, Gamma A, Hantouche E, Meyer TD, et al. The hcl-32:
507 towards a self-assessment tool for hypomanic symptoms in outpatients. J. Affect. Disord.
508 2005;88:217-33. doi:10.1016/j.jad.2005.05.011.
509 43. McIntyre RS, Cha DS, Soczynska JK, Woldeyohannes HO, Gallaugher LA, Kudlow P, et al.
510 Cognitive deficits and functional outcomes in major depressive disorder: determinants, substrates,
511 and treatment interventions. Depress. Anxiety. 2013;30:515-27. doi:10.1002/da.22063.
512 44. Lam RW, Kennedy SH, McIntyre RS, Khullar A. Cognitive dysfunction in major depressive

513 disorder: effects on psychosocial functioning and implications for treatment. Can. J. Psychiatry Rev.
514 Can. Psychiatr. 2014;59:649-54. doi:10.1177/070674371405901206.
515 45. Lieder F, Griffiths TL. Resource-rational analysis: understanding human cognition as the
516 optimal use of limited computational resources. Behav. Brain Sci. 2020;43:e1.
517 doi:10.1017/S0140525X1900061X.
518 46. Seufert T, Hamm V, Vogt A, Riemer V. The interplay of cognitive load, learners' resources and
519 self-regulation. Educ. Psychol. Rev. 2024;36:50. doi:10.1007/s10648-024-09890-1.
520 47. Corbetta M, Shulman GL. Control of goal-directed and stimulus-driven attention in the brain.
521 Nat. Rev. Neurosci. 2002;3:201-15. doi:10.1038/nrn755.
522 48. Corbetta M, Patel G, Shulman GL. The reorienting system of the human brain: from
523 environment to theory of mind. Neuron. 2008;58:306-24. doi:10.1016/j.neuron.2008.04.017.
524 49. Jonides J, Schumacher EH, Smith EE, Koeppe RA, Awh E, Reuter-Lorenz PA, et al. The role
525 of parietal cortex in verbal working memory. J. Neurosci. 1998;18:5026-34.
526 doi:10.1523/JNEUROSCI.18-13-05026.1998.
527 50. Fell J, Axmacher N. The role of phase synchronization in memory processes. Nat. Rev.
528 Neurosci. 2011;12:105-18. doi:10.1038/nrn2979.
529 51. Herweg NA, Solomon EA, Kahana MJ. Theta oscillations in human memory. Trends Cogn.
530 Sci. 2020;24:208-27. doi:10.1016/j.tics.2019.12.006.
531 52. Lundqvist M, Rose J, Herman P, Brincat SL, Buschman TJ, Miller EK. Gamma and beta bursts
532 underlie working memory. Neuron. 2016;90:152-64. doi:10.1016/j.neuron.2016.02.028.
533 53. Bramson B, Ouden HE den, Toni I, Roelofs K. Improving emotional-action control by
534 targeting long-range phase-amplitude neuronal coupling. eLife. 2020;9:e59600.
535 doi:10.7554/eLife.59600.

536 **Tables**

537 Table 1. Demographic and clinical characteristics of participants.

Characteristic	HC (n = 35)	MDD (n = 35)	Statistic	p
Sex, female/male	22/13	17/18	χ^2 (1) = 1.447	0.229
Age, years	22.00 (20.25, 29.25)	25.00 (21.00, 30.00)	U = 529.5	0.330
Education, years	15.00 (14.00, 16.00)	15.00 (14.00, 16.00)	U = 601.5	0.900
Handedness, right/left	32/3	31/4	OR = 1.376	1.000
PHQ-9	1.00 (0.00, 4.00)	18.00 (14.00, 23.00)	U = 11.0	<0.001
GAD-7	1.00 (0.00, 2.75)	15.00 (11.25, 17.00)	U = 34.0	<0.001
HCL-32	3.00 (2.00, 5.00)	4.00 (3.00, 6.00)	U = 461.0	0.074

Continuous variables are presented as median (interquartile range), and categorical variables are presented as counts. Between-group comparisons used Mann-Whitney U tests for continuous variables, chi-square test for sex distribution, and Fisher exact test for handedness. PHQ-9, Patient Health Questionnaire-9; GAD-7, Generalized Anxiety Disorder-7; HCL-32, Hypomania Checklist-32.

Table 2. Frequency- and spatially resolved summaries of TGC interaction effects.

ROI	Analysis level	Significant tests	Mean Δinteraction	Median Δinteraction	Max |Δinteraction|	q range
LF-LP	Frequency-resolved	74/75	0.001069	0.001054	0.001684	[0.005918, 0.05156]
LF-LP	Spatially resolved	88/90	0.001031	0.001007	0.001510	[0.003622, 0.06964]
LF-RP	Frequency-resolved	75/75	0.001344	0.001321	0.001805	[0.0006403, 0.01384]
LF-RP	Spatially resolved	89/90	0.001467	0.001413	0.002562	[0.0004679, 0.05791]
RF-LP	Frequency-resolved	71/75	0.001039	0.001022	0.001473	[0.01241, 0.1135]
RF-LP	Spatially resolved	85/90	0.000963	0.000990	0.001241	[0.007825, 0.1224]
RF-RP	Frequency-resolved	75/75	0.001305	0.001303	0.001711	[0.0004531, 0.01082]
RF-RP	Spatially resolved	90/90	0.001447	0.001351	0.002517	[0.000567, 0.02451]

Frequency-resolved analyses were performed after averaging across channel pairs, with 75 theta-

546 gamma frequency pairs tested within each ROI. Spatially resolved analyses were performed after
547 averaging across frequency pairs, with 90 frontal-parietal channel pairs tested within each ROI. Delta
548 interaction was defined as (HC_4-back - HC_2-back) - (MDD_4-back - MDD_2-back).

549 **Figure Legends**

550 Figure 1. WM task paradigm.

551 Figure 2. Procedure for calculating theta-gamma phase-amplitude coupling (TGC) and the
552 modulation index (MI). The raw signal (A) was filtered separately within the frequency ranges used
553 to extract phase (B) and amplitude (D, thin line). The phase time series (C) and amplitude envelope
554 (D, thick line) were then derived from the filtered signals using the Hilbert transform. A composite
555 phase-amplitude time series was subsequently constructed to obtain the mean amplitude distribution
556 across phase bins (E; two cycles are shown for clarity).

557 Figure 3. WM performance during the 2-back and 4-back tasks. (A) Accuracy, (B) d-prime, and
558 (C) correct-response reaction time are shown for the HC group and the MDD group. Individual points
559 represent participants, and boxes summarize the group distributions. Asterisks indicate statistically
560 significant differences: *** $p < 0.001$.

561 Figure 4. Altered load-dependent modulation of ROI-averaged frontoparietal TGC in MDD. The
562 forest plot shows the group × load interaction effect for each frontoparietal pathway, expressed as
563 Δinteraction = (HC_4-back – HC_2-back) - (MDD_4-back – MDD_2-back). Error bars indicate 95%
564 confidence intervals, and positive values indicate stronger load-related TGC increases in the HC
565 group than in the MDD group. Task-wise distributions show ROI-averaged TGC for HC and MDD
566 participants during the 2-back task and the 4-back task. Panels show (A) LF-LP, (B) LF-RP, (C) RF-
567 LP, and (D) RF-RP. Asterisks indicate statistically significant differences: * $p < 0.05$, ** $p < 0.01$.

568 Figure 5. Frequency-resolved TGC interaction effects. Heatmaps show Δinteraction values for
569 each theta-gamma frequency pair within each frontoparietal pathway: (A) LF-LP, (B) LF-RP, (C) RF-
570 LP, and (D) RF-RP. Channel pairs were averaged before frequency-resolved statistical testing. Cells

labeled “n.s.” denote theta-gamma frequency pairs that were not significant after FDR correction within each ROI.

Figure 6. Spatial distribution of frontoparietal TGC interaction effects. Brain network views show the strongest 10% of FDR-significant channel-pair interaction effects within each ROI, selected only for visualization. Panels show (A) superior view, (B) posterior view, (C) left lateral view, and (D) right lateral view. The complete channel-pair interaction matrices are shown in Figure S1.

Figure 7. Control analyses for regional power and theta-band phase synchronization. Forest plots show group × load interaction effects for (A) regional theta/gamma power and (B) theta-band frontoparietal wPLI. Effect estimates are plotted with 95% confidence intervals; the vertical dashed line indicates zero. No control measure showed a significant group × goad interaction after FDR correction.

Additional file 1

File format: DOCX

Title: Supplementary tables and the complete spatial distribution of frontoparietal TGC interaction effects

Description: This file contains the complete channel-pair matrices for the spatially resolved TGC analyses and supplementary tables reporting simple effects and control analyses.

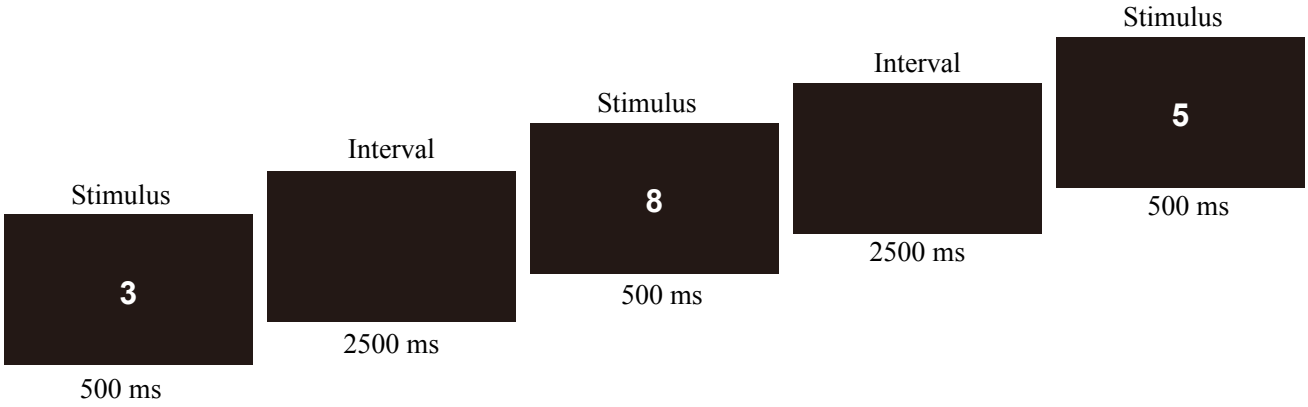
Stimulus
3
500 ms
Interval
2500 ms
Stimulus
8
500 ms
Interval
2500 ms
Stimulus
5
500 ms

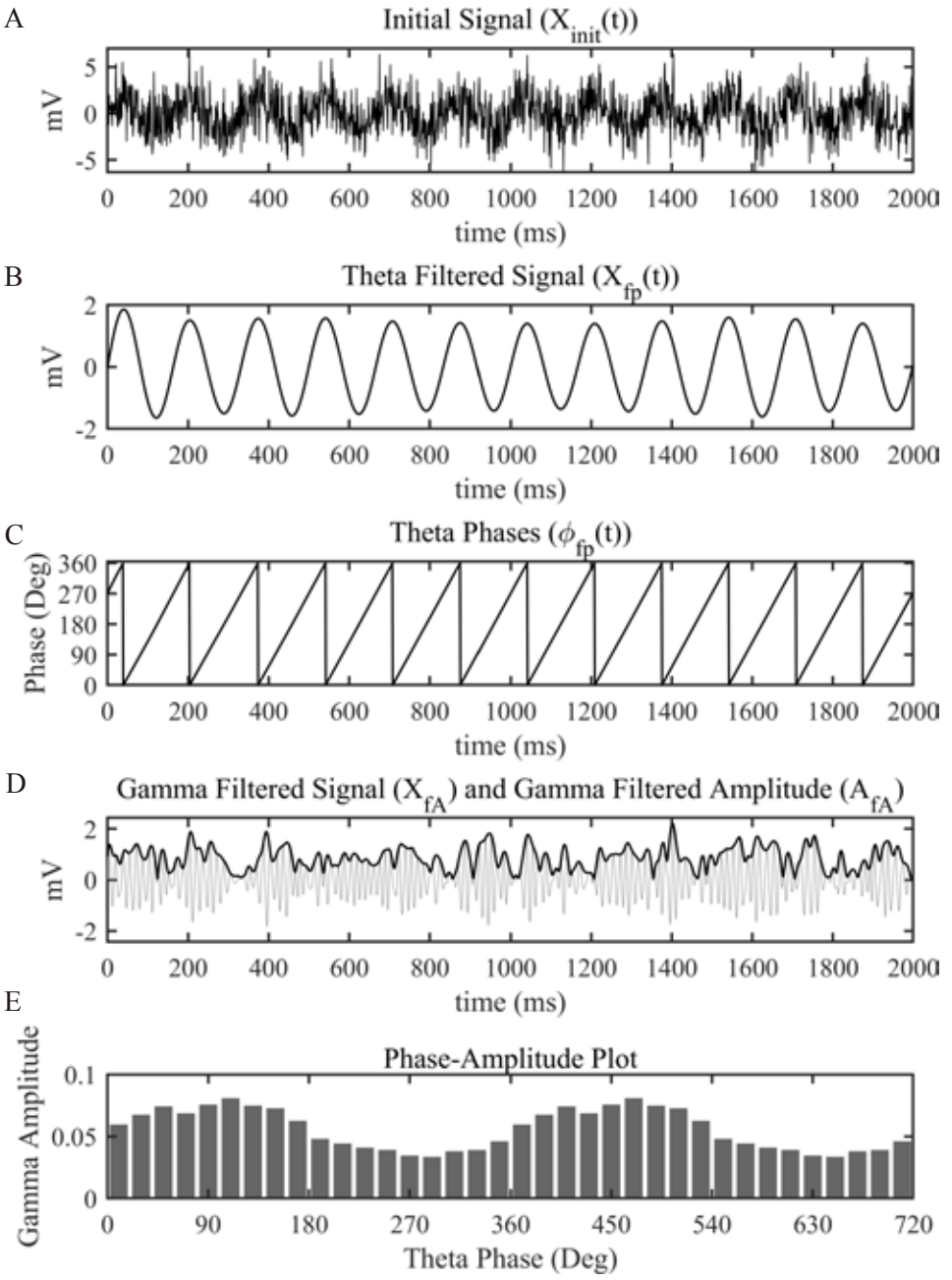
A
Initial Signal ($X_{init}(t)$)
mV
5
0
-5
0
200
400
600
800
1000
1200
1400
1600
1800
2000
time (ms)
B
Theta Filtered Signal ($X_{fp}(t)$)
mV
2
0
-2
time (ms)
C
Theta Phases ($\phi_{fp}(t)$)
Phase (Deg)
360
270
180
90
0
time (ms)
D
Gamma Filtered Signal (X_{fA}) and Gamma Filtered Amplitude (A_{fA})
mV
time (ms)
E
Phase-Amplitude Plot
Gamma Amplitude
0.1
0.05
0
0
90
180
270
360
450
540
630
720
Theta Phase (Deg)

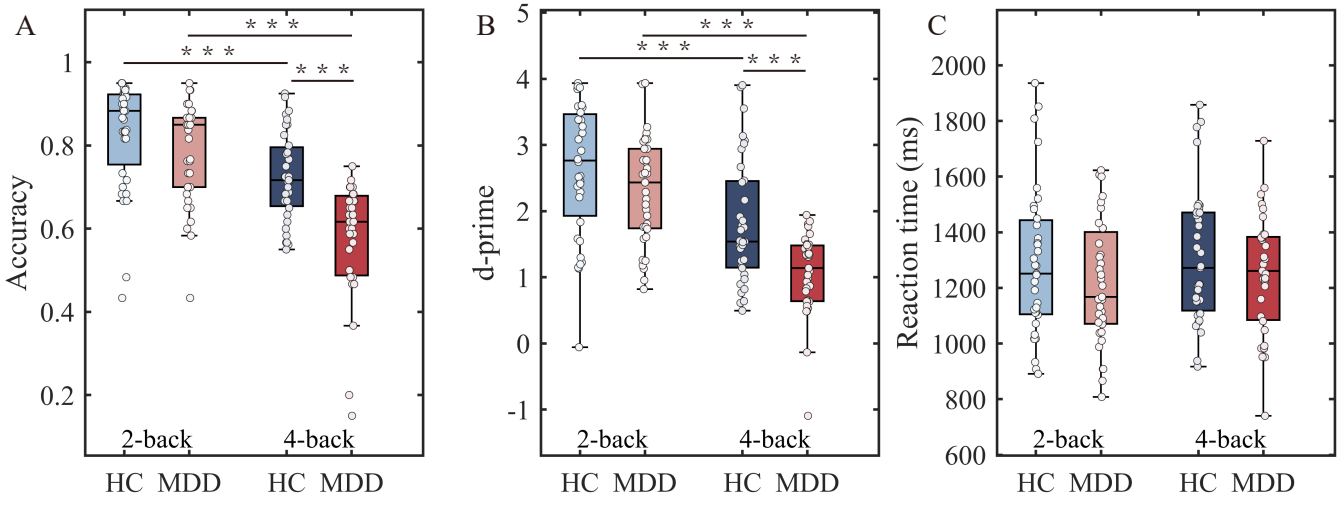
A
B
C
Accuracy
d-prime
Reaction time (ms)
* * *
2-back
4-back
HC MDD HC MDD

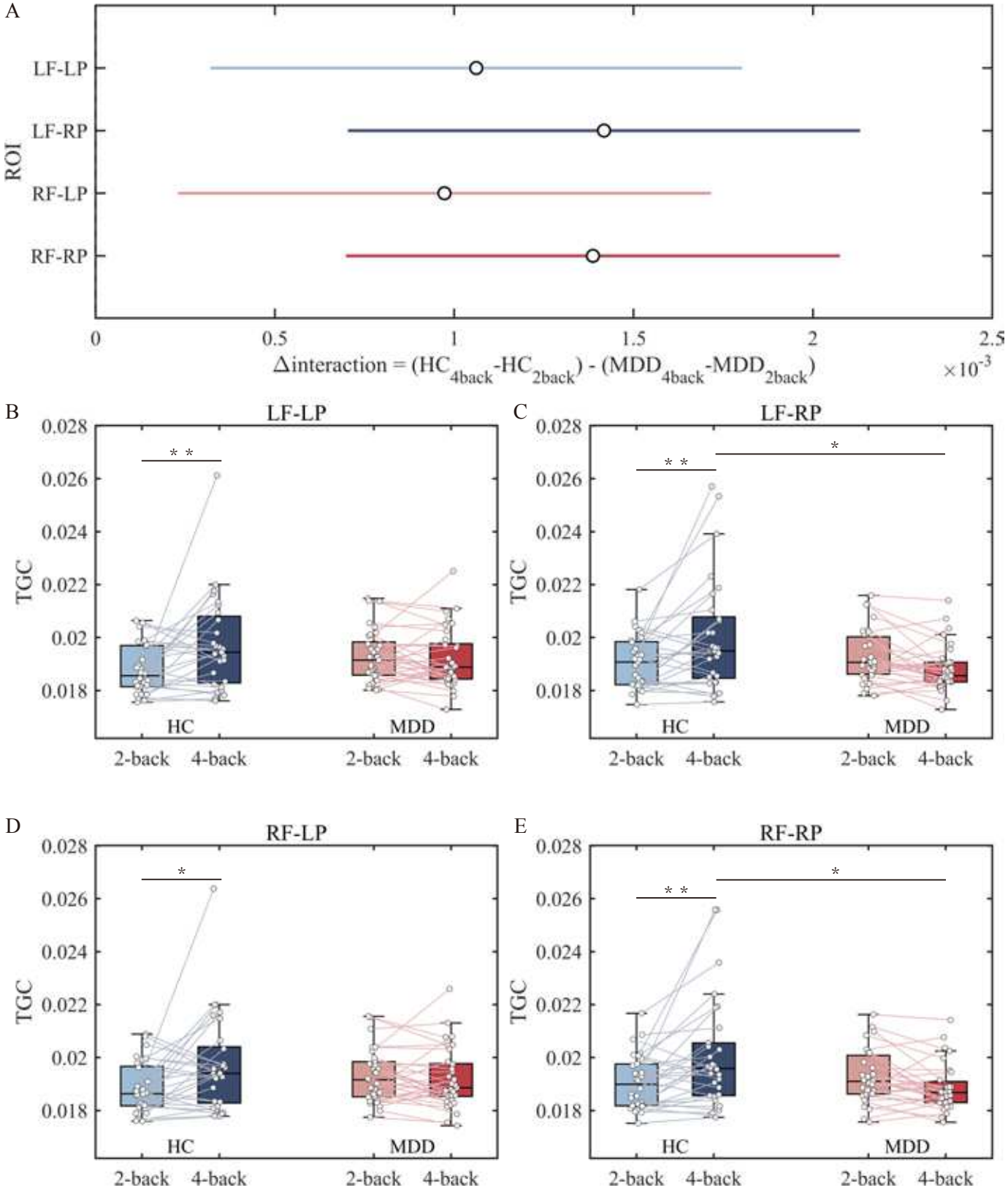
A
LF-LP
LF-RP
RF-LP
RF-RP
ROI
0
0.5
1
1.5
2
2.5
Δinteraction = (HC4back-HC2back) - (MDD4back-MDD2back)
×10-3
B
LF-LP
C
LF-RP
D
RF-LP
E
RF-RP
TGC
0.028
0.026
0.024
0.022
0.02
0.018
* *
*
HC
MDD
2-back
4-back

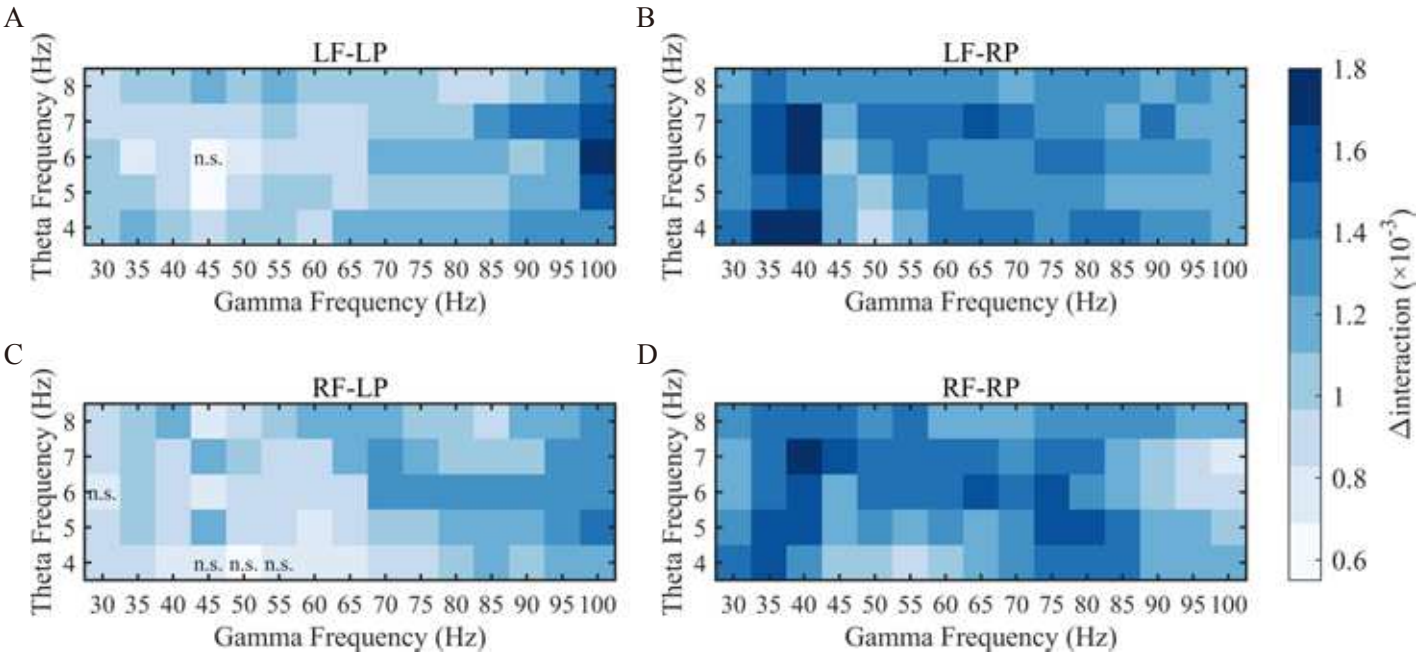
A
LF-LP
Theta Frequency (Hz)
8
7
6
5
4
n.s.
30 35 40 45 50 55 60 65 70 75 80 85 90 95 100
Gamma Frequency (Hz)
B
LF-RP
Theta Frequency (Hz)
8
7
6
5
4
30 35 40 45 50 55 60 65 70 75 80 85 90 95 100
Gamma Frequency (Hz)
1.8
1.6
1.4
1.2
1
0.8
0.6
Δinteraction (×10-3)
C
RF-LP
Theta Frequency (Hz)
8
7
6
5
4
n.s.
n.s. n.s. n.s.
30 35 40 45 50 55 60 65 70 75 80 85 90 95 100
Gamma Frequency (Hz)
D
RF-RP
Theta Frequency (Hz)
8
7
6
5
4
30 35 40 45 50 55 60 65 70 75 80 85 90 95 100
Gamma Frequency (Hz)

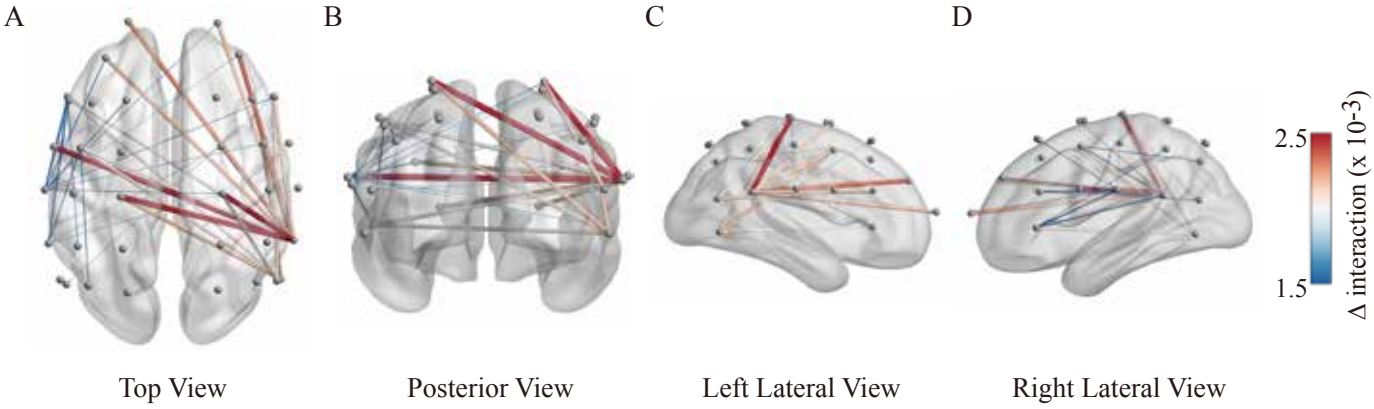
A
B
C
D
2.5
1.5
Δ interaction (x 10-3)
Top View
Posterior View
Left Lateral View
Right Lateral View

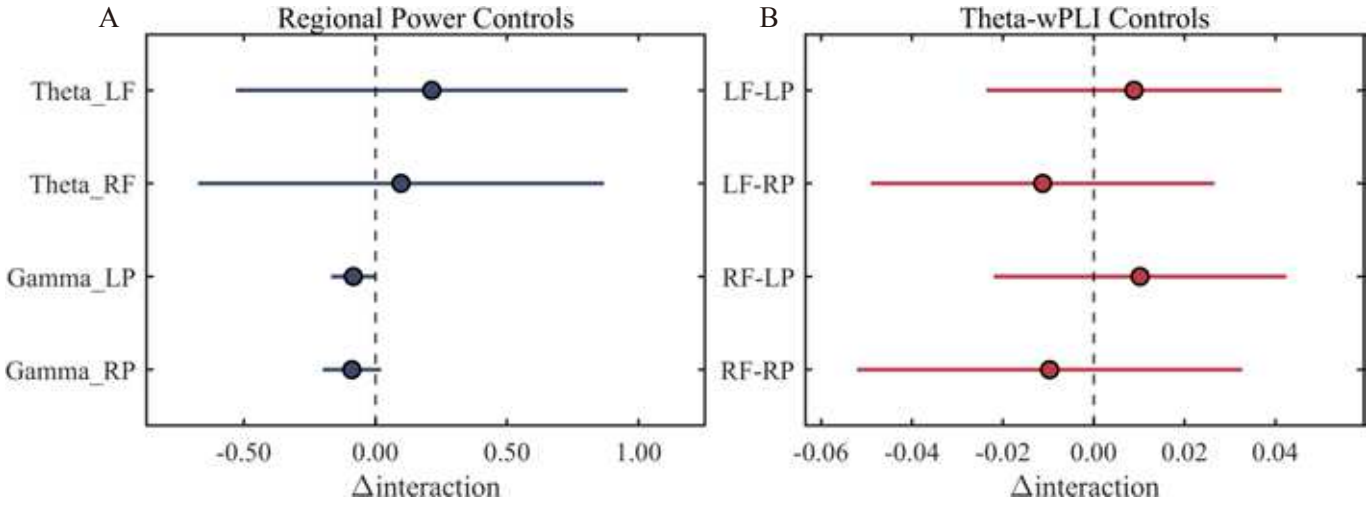
A
Regional Power Controls
Theta_LF
Theta_RF
Gamma_LP
Gamma_RP
-0.50
0.00
0.50
1.00
Δinteraction
B
Theta-wPLI Controls
LF-LP
LF-RP
RF-LP
RF-RP
-0.06
-0.04
-0.02
0.00
0.02
0.04
Δinteraction

Supplementary Files

This is a list of supplementary files associated with this preprint. Click to download.

- Additionalfile1.docx